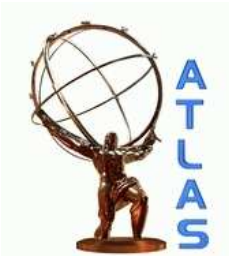

ATLAS NOTE

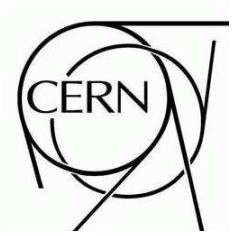

March 11, 2009

Search for Leptoquark Pairs and Majorana Neutrinos from Right-Handed W Boson Decays in Dilepton-Jets Final States

The ATLAS Collaboration[1)]

This note is part of CERN-OPEN-2008-020. This version of the note should not be cited: all citations should be to CERN-OPEN-2008-020.

ATL-PHYS-PUB-2009-072
10 May 2009

Abstract

Final states with high-p_T leptons and jets are predicted by many Beyond the Standard Model scenarios. Two prominent models are used here as guides to understanding the event topologies: the scalar leptoquarks and the Left-Right Symmetry. In contrast to many SUSY signatures, their topologies rarely contain missing energy. Their discovery potential with early ATLAS data, corresponding to an integrated luminosity of a few hundred inverse picobarns, is discussed.

[1)] V. Bansal, C. Boulahouache, G. Krobath, E. Panagiotopoulou, T. Papadopoulou, V. Savinov, R. Ströehmer, G. Unel, S. Wendler.

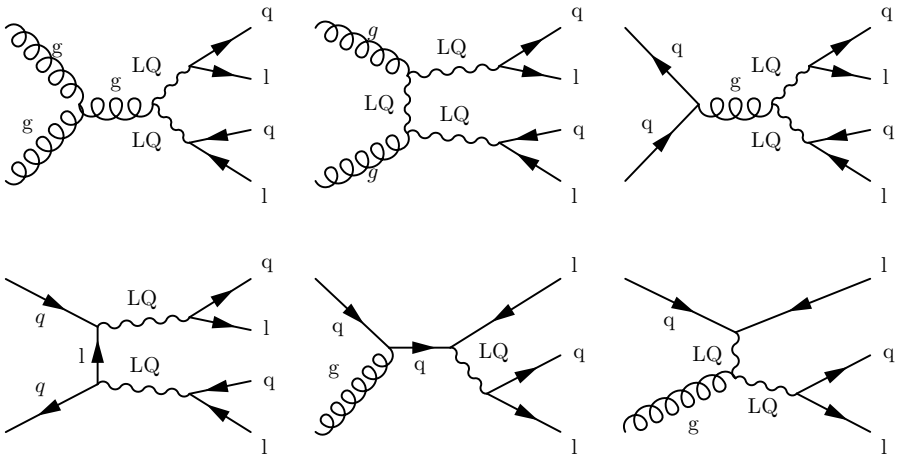

Figure 1: Feynman diagrams for leptoquark production.

1 Introduction

Grand Unification has inspired many extensions of the Standard Model. Such models introduce new, usually very heavy particles, and previous searches for Grand Unification Theory (GUT) signatures have placed limits on masses and interaction strengths of the new particles. The LHC will probe new regions of parameter space, allowing for a direct search for these particles. Decays characterized by final states with two highly energetic leptons, two jets and no missing transverse energy are studied in this note. The models for new physics considered for this note are described below. The simulation of signal and background processes is described in section 2. In section 4 the baseline selection that is used for all analyses is explained. After the trigger requirements are given (section 3), section 5 details the specifics of each of the analyses. The systematics are described in section 6 and the final sensitivity estimates are given in section 7.

1.1 Leptoquarks

The experimentally observed symmetry between leptons and quarks has motivated the search for leptoquarks (LQ), hypothetical bosons carrying both quark and lepton quantum numbers, as well as fractional electric charge [1–5]. Leptoquarks could, in principle, decay into any combination of a lepton and a quark. Experimental limits on lepton number violation, flavor-changing neutral currents, and proton decay favour three generations of leptoquarks. In such a scenario, each leptoquark couples to a lepton and a quark from the same Standard Model generation [6]. Leptoquarks can either be produced in pairs by the strong interaction or in association with a lepton via the leptoquark-quark-lepton coupling. Figure 1 shows the Feynman diagrams for leptoquark production processes accessible at the LHC.

This note describes the search for leptoquarks decaying to either an electron and a quark or a muon and a quark. The branching ratio of a leptoquark to a charged lepton and a quark is denoted as β. Decays to neutrinos are not considered, and events are not explicitly selected based on the flavor of the quark. The experiments at the Tevatron have searched for first (decaying to eq), second (decaying to μq), and third (decaying to τq) generation scalar leptoquarks. For $\beta = \mathscr{B}(LQ \to \ell^{\pm} q) = 1$, the DØ [7] and CDF [8] collaborations have set 95%CL limits for first generation scalar leptoquarks of $m_{\mathrm{LQ}_1} > 256$ GeV and $m_{\mathrm{LQ}_1} > 236$ GeV, respectively. These limits are based on integrated $p\bar{p}$ luminosities of approxi-

mately 250 pb^{-1} and 200 pb^{-1}. The results for second generation leptoquarks, $m_{\mathrm{LQ}_2} > 251$ GeV and $m_{\mathrm{LQ}_2} > 226$ GeV, were obtained with 300 pb^{-1} and 200 pb^{-1} by the DØ [9] and CDF [10] experiments, respectively.

The Tevatron exclusion limits are expected to reach 300-350 GeV in the near future.

1.2 Left-Right Symmetry

Left-Right Symmetric Models (LRSMs) of the weak interaction address two important topics: the nonzero masses of the three known left-handed neutrinos [11] and baryogenesis. LRSMs conserve parity at high energies by introducing three new heavy right-handed Majorana neutrinos N_e, N_μ and N_τ. The smallest gauge group that implements an LRSM is $SU(2)_L \times SU(2)_R \times U(1)_{B-L}$. At low energies, the left-right symmetry is broken and parity is violated. The Majorana nature of the new heavy neutrinos explains the masses of the three left-handed neutrinos through the see-saw mechanism [12]. The lepton number L could be violated in processes that involve the Majorana neutrinos. This opens a window to the very attractive theoretical scenario for baryogenesis via leptogenesis, where baryon and lepton numbers B and L are violated but $B-L$ is conserved.

In addition to the Majorana neutrinos, most general LRSMs also introduce the new intermediate vector bosons W_R and Z', Higgs bosons, and a left-right mixing parameter. The most restrictive lower limit on the mass of the W_R boson comes from the $K_L - K_S$ mass difference which requires $m_{W_R} >$ 1.6 TeV. This lower limit is subject to large corrections from higher-order QCD effects. Heavy right-handed Majorana neutrinos with masses of about a few hundred GeV would be consistent with the data from supernova SN1987A. Such heavy neutrinos would allow for a W_R boson at the TeV mass scale. This scenario would also be consistent with LEP data on the invisible width of the Z boson. Present experimental data on neutral currents imply a lower limit on the mass of a Z' boson of approximately 400 GeV. Recent direct searches [13] for the W_R boson at DØ give a lower mass limit of 739 GeV and 768 GeV, assuming the W_R boson could decay to both lepton pairs and quark pairs, or only to quark pairs, respectively. However, heavy Majorana neutrinos decaying to a lepton and a pair of quarks (detected as jets) were not searched for in those analyses.

The new intermediate vector bosons W_R and Z' would be produced at the LHC via the Drell-Yan (DY) process like Standard Model W and Z bosons. Their decays would be a source of new Majorana neutrinos. The Feynman diagram for W_R boson production and its subsequent decay to a Majorana neutrino is shown in Fig. 2. This note describes an analysis of W_R boson production and its decays $W_R \to eN_e$ and $W_R \to \mu N_\mu$, followed by the decays $N_e \to eq'\bar{q}$ and $N_\mu \to \mu q'\bar{q}$, which can be detected in final states with (at least) two leptons and two jets.

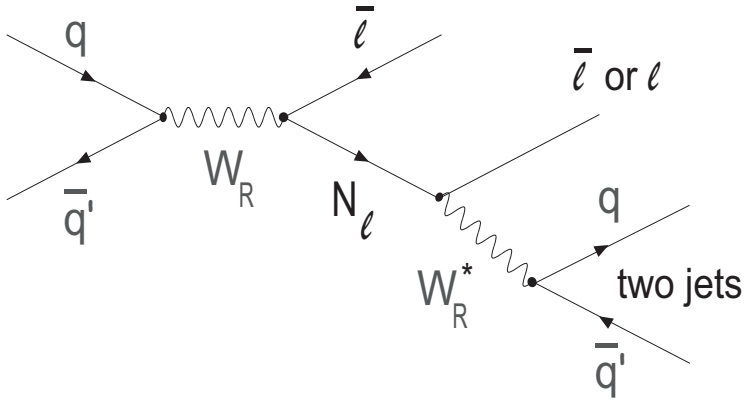

Figure 2: Feynman diagram for W_R boson production and its decay to a Majorana neutrino N_ℓ.

m_{LQ} in GeV	$\sigma(pp \to LQ\bar{LQ})$ (NLO) in pb
300	10.1 ± 1.5
400	2.24 ± 0.38
600	0.225 ± 0.048
800	0.0378 ± 0.0105

Table 1: NLO cross-sections for scalar leptoquark pair production at the LHC [16].

2 Simulation of Physics Processes

2.1 Leptoquarks

The signals have been studied using samples of first generation (1st gen.) and second generation (2nd gen.) scalar leptoquarks simulated with the Monte Carlo (MC) generator PYTHIA [14] and using the CTEQ6L1 parameterization [15] of the parton density functions (PDFs). A leptoquark-lepton-quark coupling $\lambda = 0.8$ was used in the event generation leading to a natural width of the leptoquarks of 0.63 GeV and 1.3 GeV for leptoquark masses of 400 GeV and 800 GeV respectively. The next to leading order (NLO) cross-sections for leptoquark pair production at 14 TeV pp centre-of-mass energy were taken from Ref. [16] and are shown in Table 1 for the four simulated leptoquark masses.

2.2 Left-Right Symmetry

Studies of the discovery potential for W_R bosons and the Majorana neutrinos, N_e and N_μ produced in their decays, were performed using datasets simulated with the MC generator PYTHIA according to a particular implementation [17] of an LRSM described in [18]. The Standard Model axial and vector couplings, the CKM matrix for the quark sector, no mixing between the new and Standard Model intermediate vector bosons, and phase space isotropic decays of Majorana neutrinos are assumed for the right-handed sector in this model. The products of leading-order production cross-sections $\sigma(pp \to W_R X)$ and branching fractions to studied final states $W_R \to \ell N_\ell \to \ell\ell jj$ are 24.8 pb for $m_{W_R} = 1800$ GeV, $m_{N_e} = m_{N_\mu} = 300$ GeV and 47.0 pb for $m_{W_R} = 1500$ GeV, $m_{N_e} = m_{N_\mu} = 500$ GeV. In the rest of this note, these samples are referred to as LRSM_18_3 and LRSM_15_5, respectively. The Majorana nature of the new heavy neutrinos allows for same-sign and opposite-sign dileptons.

2.3 Background Processes

The main sources of background for the analyses presented here are $t\bar{t}$ and inclusive Z/γ^* production processes. Multijet production, where two jets are misidentified as leptons, represents another background. In addition, minor contributions arise from diboson production. Other potential background sources, such as single-top production, were also studied. Their contribution was found to be insignificant.

- Z/γ^* background was studied using a combination of two MC samples with generator-level dilepton invariant mass preselections of $m_{\ell\ell} > 60$ GeV and $m_{\ell\ell} > 150$ GeV, the latter sample corresponding to a much larger integrated luminosity than the former. The samples were normalized to the given luminosity using their partial cross-sections and the NLO estimate $\sigma(pp \to Z) \times \mathscr{B}(Z \to \ell^+\ell^-) = 2032$ pb, obtained with the MC generator FEWZ [19, 20]. A lepton filter was applied at the event generation, requiring at least one electron or muon with transverse momentum greater than 10 GeV and absolute pseudo-rapidity smaller than 2.7, resulting in an effective cross-section of 1808 pb.

For logistical reasons, the sample with the lower mass preselection was generated using the MC generator PYTHIA [14], and the sample with higher mass preselection was generated using HERWIG [21]. In both cases, the CTEQ6L1 [15] parton distribution functions were used. The consistency between the two samples was verified at high dilepton masses.

- $t\bar{t}$ background was simulated using the MC generator MC@NLO [22] using the CTEQ6M [15] parton distribution functions. It was normalized to the given integrated luminosity using a production cross-section of 833 pb estimated to the next-to-leading order (NLO+NLL) [23]. In addition, a lepton filter was applied, requiring at least one electron or muon with transverse momentum greater than 1 GeV, which resulted in an effective cross-section of 450 pb.

- The diboson samples were generated using HERWIG with a generator-level preselection on the invariant mass of $Z/\gamma^* > 20$ GeV. With this requirement, the NLO partial cross-sections for WW, WZ and ZZ boson pair production processes were numerically estimated (using MC@NLO) to be 117.6 pb, 56.4 pb, 17.8 pb, respectively. The CTEQ6L1 parton distribution functions were used for event generation. Again, a lepton filter was applied, with a transverse momentum threshold of 10 GeV and a maximum absolute pseudo-rapidity of 2.8. This resulted in a total effective cross-section of 60.9 pb.

- The multijet background was simulated using PYTHIA with the CTEQ6L1 structure functions. The normalization was based on PYTHIA cross-section estimates. The statistics of these samples are very limited, such that no reliable estimate of this background could be made at this time.

3 Trigger Requirements

The trigger system [24] of the ATLAS experiment has three levels, L1, L2 and the Event Filter (EF). To ensure high overall trigger efficiencies, our analyses rely on single lepton trigger streams with relatively low thresholds. The dielectron analyses rely on the single electron-based trigger called `e55` which has a threshold of around 60 GeV [24]. When selected events fail this trigger, the analyses rely on the lower-threshold (about 25 GeV) single electron trigger called `e22i` [24] in which the electron is required to be isolated. A single muon trigger with threshold about 20 GeV (`mu20` [24]) is used in the dimuon analyses.

Final states studied in this note always contain two high-p_T leptons. While the baseline selection described in section 4 requires two leptons with $p_T > 20$ GeV, most signal events contain at least one lepton with significantly higher p_T. As a result, the overall trigger efficiency for events that satisfy all analysis selection criteria (section 5) exceeds 95%. The trigger efficiencies for signal MC events that satisfy all selection criteria are shown in Table 2.

Process	L1	L2	EF	L1*L2*EF
1st gen. leptoquarks $m_{LQ} = 400$ GeV	100.0%	99.4%	97.6%	97.0%
2nd gen. leptoquarks $m_{LQ} = 400$ GeV	97.7%	99.1%	99.7%	96.5%
LRSM (ee) $m_{W_R} = 1800$ GeV, $m_{N_e} = 300$ GeV	100.0%	99.2%	97.2%	96.4%
LRSM ($\mu\mu$) $m_{W_R} = 1800$ GeV, $m_{N_\mu} = 300$ GeV	96.8%	98.7%	98.9%	94.5%

Table 2: Overall trigger efficiencies for signal events that satisfy all selection criteria.

4 Baseline Event Selection

The baseline event selection, common for all analyses presented in this note, requires two leptons and two jets. All analyses use the same selection criteria for signal electron, muon, and jet candidates. The baseline selection criteria for these reconstructed objects are summarized below. Performance studies are described elsewhere [25–28].

Electron candidates are identified as energy clusters reconstructed in the liquid argon electromagnetic calorimeter that match tracks reconstructed in the inner tracking detector and satisfy the *medium* electron identification requirements [25].

Muon candidates are identified as tracks reconstructed in the muon spectrometer [26] that, when extrapolated to the beam axis, match a track reconstructed in the inner detector, and satisfy relative isolation energy requirements $E_T^{iso}/p_T^{\mu} \leq 0.3$. p_T^{μ} is the muon candidate's transverse momentum and E_T^{iso} is the energy detected in the calorimeters in a cone of $\Delta R=\sqrt{\Delta\eta^2+\Delta\phi^2}=0.2$ around the muon candidate's reconstructed trajectory, corrected for the expected energy deposition by a muon.

Jets are identified as energy clusters reconstructed in the calorimeters using a $\Delta R=0.4$ cone algorithm [27]. ΔR between a jet and any electron candidate (as defined above) must be larger than 0.1. This veto is imposed to avoid electrons being misidentified as jets. It is applied in all analyses, regardless of whether electrons are explicitly considered in the final states or not. The jet energy scale calibration is performed using full MC simulation and requires that the average reconstructed jet energy agrees with the average energy of the jets reconstructed with the Monte Carlo truth particles. The same jet reconstruction algorithm, with cone size $\Delta R = 0.4$, is used for both reconstruction and calibration.

All objects are required to have $p_T \geq 20$ GeV, the leptons must have an absolute pseudo-rapidity $|\eta|$ smaller than 2.5 and jets must have $|\eta| \leq 4.5$.

To suppress contributions from Drell-Yan backgrounds, the dilepton invariant mass is required to be at least 70 GeV. Tighter analysis-specific requirements are later applied to this and other variables in order to achieve the best sensitivities in individual studies, as described in the following section.

5 Individual Analyses

5.1 Search for Leptoquark Pair Production

Following the baseline object identification criteria described above, the leptoquark pair analyses require events to have at least two oppositely charged leptons of the same flavour and at least two jets. Signal sensitivity and discovery potential are estimated using a sliding mass window algorithm: only events in the mass region around the assumed mass of the leptoquark are analyzed.

For large leptoquark masses, signal leptons and jets have, on average, larger transverse momenta than background particles. The following kinematic quantities are used to separate the signal from backgrounds: the transverse momentum of the leptons (p_T), the scalar sum of the transverse momenta of the two most energetic jets and leptons ($S_T = \sum|\vec{p}_T|_{jet} + \sum|\vec{p}_T|_{lep}$), the dilepton invariant mass ($m_{\ell\ell}$), and lepton-jet invariant mass. The lepton-jet invariant mass represents the mass of the leptoquark if the correct lepton-jet combination is chosen. Since there are two leptons and two jets there are two possible combinations, and we choose the combination which gives the smallest difference between the masses of the first and second leptoquark candidates.

In both channels, the values of these selection criteria are optimized[2)] to achieve discovery with 5σ significance at the lowest luminosity possible. Tables 3 and 4 show the values of the selection criteria and resulting signal and background cross-sections for 1st and 2nd generation channels, respectively. One important difference between the two channels is the background due to jets being misidentified

[2)] At this stage, only statistical uncertainties are taken into account.

Physics sample	Before selection	Baseline selection	$S_T \geq$ 490 GeV	$m_{ee} \geq$ 120 GeV	m^1_{lj} - m^2_{lj} window (GeV)	
					[320-480] - [320-480]	[700-900] - [700-900]
LQ ($m = 400$ GeV)	2.24	1.12	1.07	1.00	0.534	-
LQ ($m = 800$ GeV)	0.0378	0.0177	0.0177	0.0174	-	0.0075
$Z/\gamma^* \geq 60$ GeV	1808.	49.77	0.722	0.0664	0.0036	0.00045
$t\bar{t}$	450.	3.23	0.298	0.215	0.0144	< 0.0012
Vector Boson pairs	60.9	0.610	0.0174	0.00384	< 0.002	< 0.0014
Multijet	10^8	20.51	0.229	0.184	0.0	0.0

Table 3: 1st generation leptoquark analysis. Partial cross-sections (pb) that survive selection criteria. The upper limits are given at 68% confidence level.

Physics sample	Before selection	Baseline selection	$p^{\mu}_T \geq$60 GeV $p^{jet}_T \geq$25 GeV	$S_T \geq$ 600 GeV	$m_{\mu\mu} \geq$ 110 GeV	m_{lj} window (GeV)	
						[300-500]	[600-1000]
LQ (400 GeV)	2.24	1.70	1.53	1.27	1.23	0.974	-
LQ (800 GeV)	0.0378	0.0313	0.0306	0.0304	0.030	-	0.0217
$Z/\gamma^* \geq$60 GeV	1808.	79.99	2.975	0.338	0.0611	0.021	0.014
$t\bar{t}$	450.	4.17	0.698	0.0791	0.0758	0.0271	0.0065
VB pairs	60.9	0.876	0.0654	0.00864	0.00316	0.00185	0.00076
Multijet	10^8	0.0	0.0	0.0	0.0	0.0	0.0

Table 4: 2nd generation leptoquark analysis. Partial cross-sections (pb) that survive selection criteria.

as electrons. This background can be significantly reduced by requiring both reconstructed jet-electron masses, (m^1_{lj}, m^2_{lj}), to be close to the tested leptoquark mass. However, such a selection in the 2nd generation analysis would significantly reduce the signal efficiency, especially for larger leptoquark masses. Therefore, a less strigent selection is applied, and only the average of the two muon-jet masses (m^{av}_{lj}) is required to be near the tested leptoquark mass.

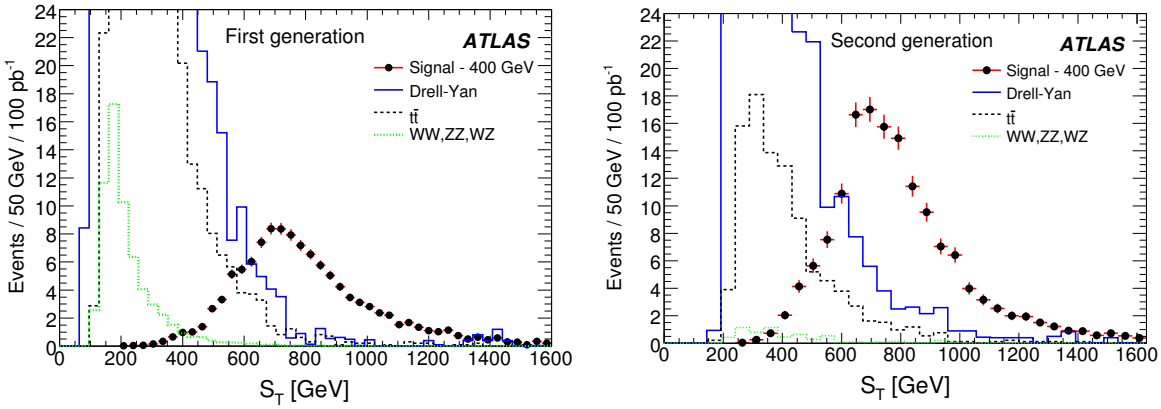

Figure 3: S_T in leptoquark MC events ($m_{LQ} = 400$ GeV) after baseline selection. Left: 1st generation, right: 2nd generation with the additional requirements $p^{\mu}_T > 60$ GeV and $p^{jet}_T > 25$ GeV.

Figure 3 shows the S_T variable distribution with $m_{LQ} = 400$ GeV, along with the main backgrounds, Drell-Yan and $t\bar{t}$ production, after baseline selection plus, for the 2nd generation case, the requirements $p_T^{\mu} > 60$ GeV and $p_T^{jet} > 25$ GeV.

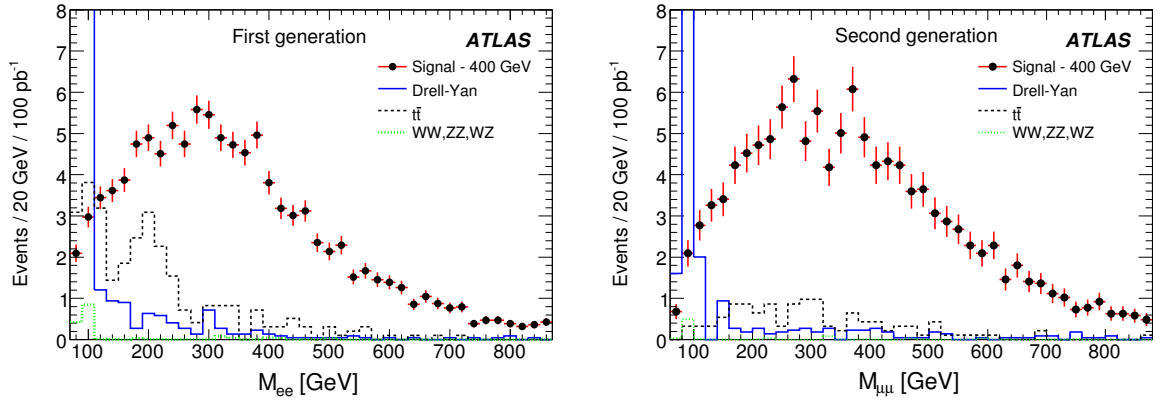

Figure 4: $m_{\ell\ell}$ of the selected lepton pair after S_T selection in leptoquark 1st generation (left) and 2nd generation (right) events ($m_{LQ} = 400$ GeV).

The dilepton mass distribution after the S_T selection is shown in Figure 4.

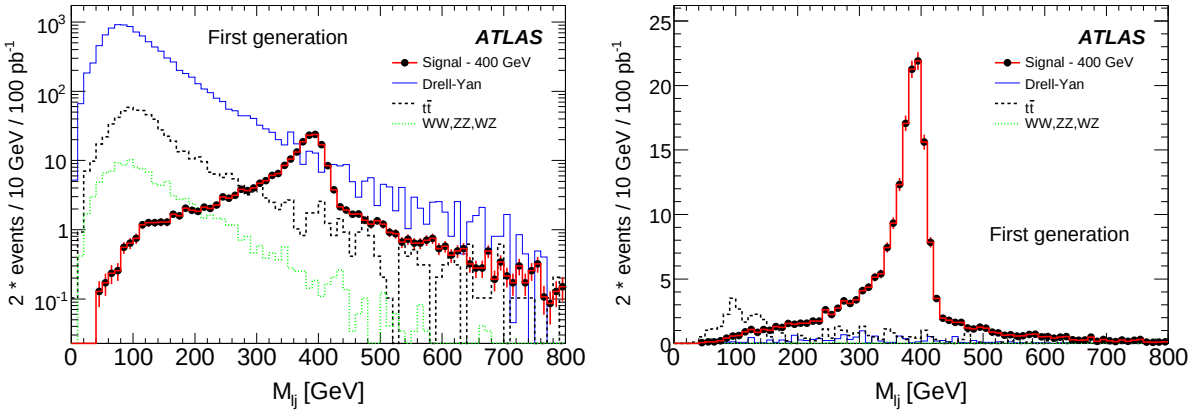

Figure 5: Reconstructed electron-jet invariant mass in the 1st generation leptoquark (m_{LQ}=400 GeV) analysis for signal and background MC events after baseline selection (left) and after all selection criteria (right). All distributions are given for 100 pb^{-1} of integrated luminosity.

Figures 5 and 6 show the reconstructed invariant mass of leptoquark candidates (m_{LQ}=400 GeV) in signal events and the main backgrounds, Drell-Yan and $t\bar{t}$ production, after the subsequent selections on dimuon mass and S_T. Due to gluon radiation, quarks produced in the decays of heavy particles are not equivalent to standard jets. This shifts the peak of the jet energy resolution function towards smaller energies and results in a low-mass shoulder in the distribution of reconstructed masses of heavy particles. Figure 5 shows two entries per event corresponding to the two reconstructed electron-jet objects obtained by adding x and y mass projections of (m_{lj}^1, m_{lj}^2) on a common axis, m_{lj}.

All figures show predicted distributions for an integrated luminosity of 100 pb^{-1}.

The trigger efficiency is not included in the plots and tables shown in this section. However events satisfying all selection criteria would trigger with an efficiency exceeding 95%, as discussed in Section 3.

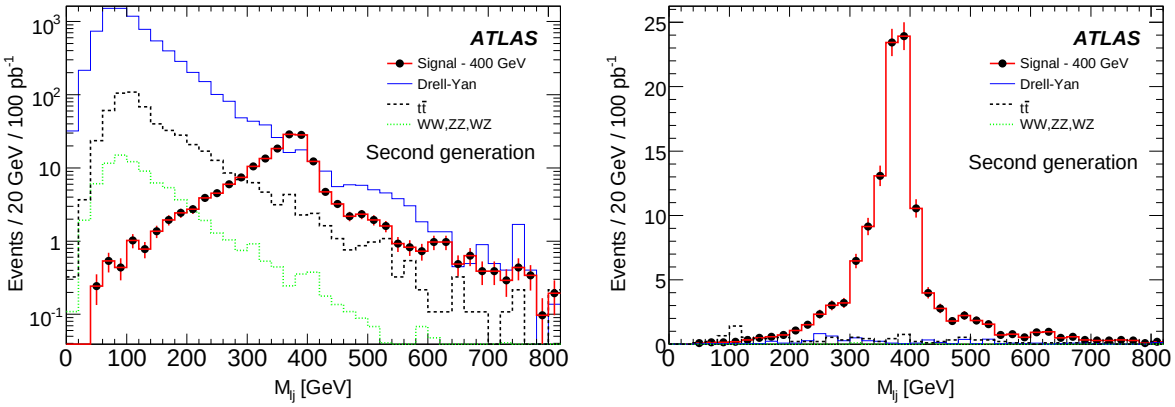

Figure 6: Reconstructed muon-jet invariant mass for 2nd generation leptoquarks (m_{LQ} = 400 GeV) in signal and background MC events after baseline selection (left) and after all selection criteria (right). All distributions are given for 100 pb^{-1} of integrated luminosity.

5.2 Search for New Particles from Left-Right Symmetric Models

Signal event candidates are required to contain (at least) two electron or muon candidates and two or more jets that pass the baseline selection criteria. As previously described, the minimum separation between a jet and an electron candidate $\Delta R \geq 0.1$ is required. The two leading p_T lepton candidates and the two leading p_T jets are assumed to be the decay products of the W_R boson. The signal jet candidates are combined with each signal lepton, and the combination that gives the smallest invariant mass is considered as the heavy neutrino (N_ℓ in Fig. 2). This assignment is correct in more than 99% of signal MC events. The other lepton is assumed to come directly from the decay of the W_R boson.

When the W_R boson is at least twice as heavy as the Majorana neutrino, the daughter lepton from the neutrino's decay often begins to partially merge with one of the daughter jets. In the dielectron analysis, when the separation between this lepton and a signal jet candidate is in the range $0.1 \leq \Delta R \leq 0.4$, using all three reconstructed objects to estimate the invariant mass of the neutrino would often result in double-counting. To solve this problem, signal event candidates in the dielectron analysis are divided into two groups. When the separation is outside the discussed range, *i.e.* $\Delta R > 0.4$, all three objects are used. However, when the separation is in the critical range, *i.e.* $0.1 \leq \Delta R \leq 0.4$, only jets are used to estimate the mass of the N_e neutrino. It must be noted that this procedure has little effect on the N_e neutrino mass resolution, because it is dominated by the resolution on the jets energy. The fraction of events falling in the critical range depends on the ratio of W_R boson and Majorana neutrino masses, and increases with this ratio, being 8% for the 1500 GeV to 500 GeV ratio and 26% for the 1800 GeV to 300 GeV ratio considered here. No such problem exists in the dimuon analysis because muon reconstruction is possible even when the reconstructed trajectory's projection into the calorimeters randomly coincides with jet activity. The mass of the Majorana neutrino can be reconstructed with a relative resolution of about 6%, and the mass of the W_R boson can be reconstructed with a relative resolution of 5% to 8%; better resolution on the latter is achieved in the dielectron analyses because the muon spectrometer resolution is degraded at high transverse momenta.

While the main background sources in LRSM analyses are $t\bar{t}$, Z/γ^*, and vector boson pair production processes, multijets were also identified as a source of potentially dangerous background in the dielectron analysis. The distributions of the scalar sum of signal object candidates' transverse momenta S_T, and the reconstructed dilepton invariant mass $m_{\ell\ell}$ for signal and background events, normalized to an integrated luminosity of 100 pb^{-1}, are shown in Figs. 7 and 8.

The choice of the selection criteria $S_T \geq 700$ GeV and $m_{\ell\ell} \geq 300$ GeV is made in order to maintain

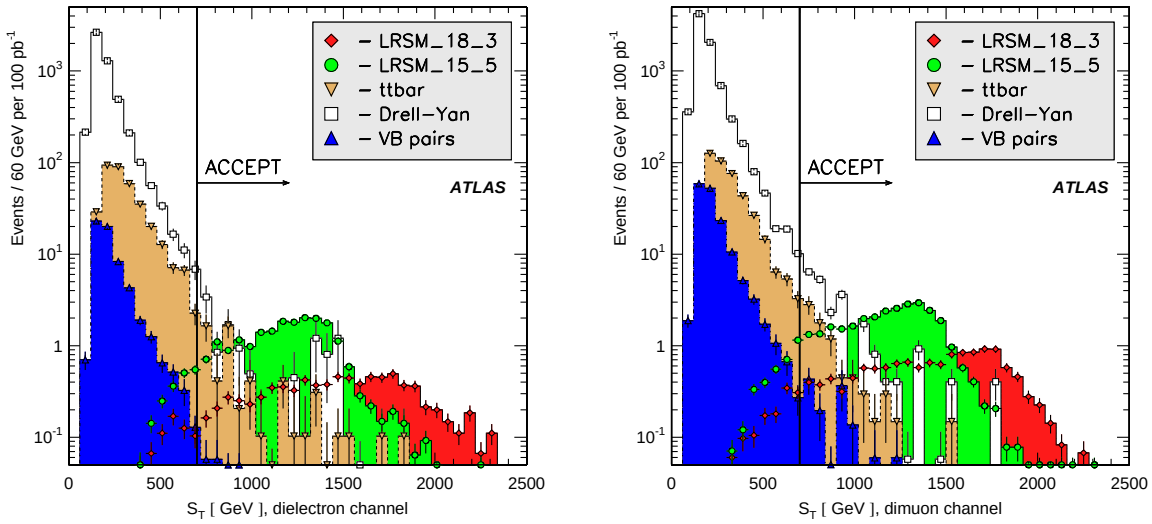

Figure 7: LRSM analysis. S_T distributions for signals and backgrounds normalized to 100 pb^{-1} of integrated luminosity after baseline selection in dielectron (left) and dimuon (right) analyses. Vertical lines indicate the region used in the analysis.

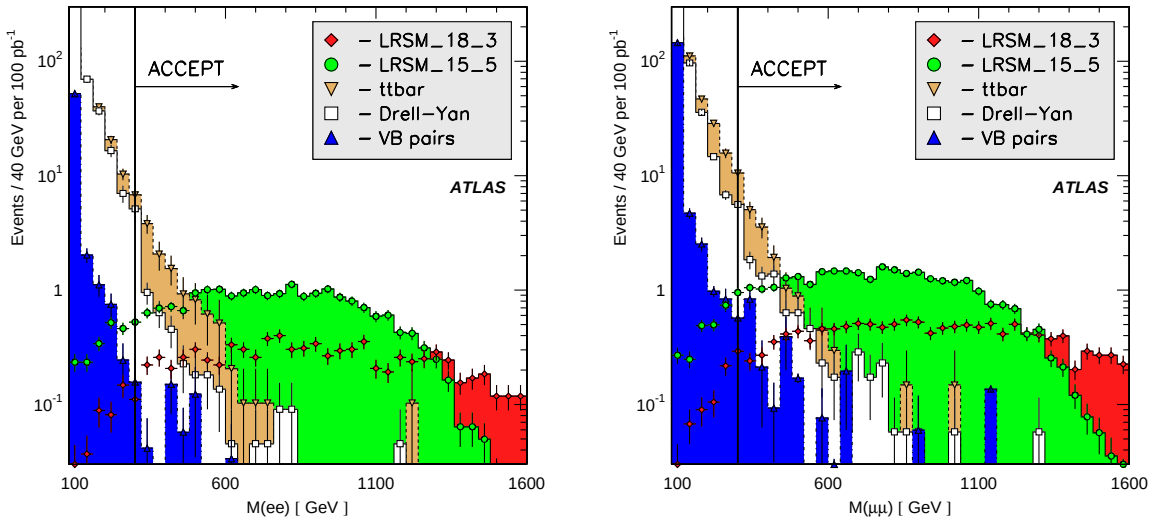

Figure 8: LRSM analysis. The distributions of $m_{\ell\ell}$ for signals and backgrounds normalized to 100 pb^{-1} of integrated luminosity after baseline selection in dielectron (left) and dimuon (right) analyses. Vertical lines indicate the region used in the analysis.

good efficiency not only for mass values used in this study, but also for signals with $m_{W_R} \geq 1000$ GeV.

Partial cross-sections for signal and background processes passing the selection criteria are shown in Tables 5 and 6. Some remarks are in order concerning the selection criteria's efficiencies. First, the dimuon channel is more efficient than the dielectron channel. This is due to the jet-electron merging

Physics sample	Before selection	Baseline selection	m_{ejj} ≥ 100 GeV	m_{eejj} ≥ 1000 GeV	m_{ee} ≥ 300 GeV	S_T ≥ 700 GeV
LRSM_18_3	0.248	0.0882	0.0882	0.0861	0.0828	0.0786
LRSM_15_5	0.470	0.220	0.220	0.215	0.196	0.184
$Z/\gamma^*, m \geq 60$ GeV	1808.	49.77	43.36	0.801	0.0132	0.0064
$t\bar{t}$	450.	3.23	3.13	0.215	0.0422	0.0165
VB pairs	60.9	0.610	0.522	0.0160	0.0016	0.0002
Multijet	10^8	20.51	19.67	0.0490	0.0444	0.0444

Table 5: LRSM dielectron analysis. Partial cross-sections (pb) that survive the selection criteria.

Physics sample	Before selection	Baseline selection	$m_{\mu jj}$ ≥ 100 GeV	$m_{\mu\mu jj}$ ≥ 1000 GeV	$m_{\mu\mu}$ ≥ 300 GeV	S_T ≥ 700 GeV
LRSM_18_3	0.248	0.145	0.145	0.141	0.136	0.128
LRSM_15_5	0.470	0.328	0.328	0.319	0.295	0.274
$Z/\gamma^*, m \geq 60$ GeV	1808.	79.99	69.13	1.46	0.0231	0.0127
$t\bar{t}$	450.	4.17	4.11	0.275	0.0527	0.0161
VB pairs	60.9	0.876	0.824	0.0257	0.0047	0.0015
Multijet	10^8	0.0	0.0	0.0	0.0	0.0

Table 6: LRSM dimuon analysis. Partial cross-sections (pb) that survive selection criteria.

discussed previously. This issue becomes especially important for a larger ratio of masses m_{W_R}/m_{N_e}. However, for a very heavy W_R boson, the dielectron channel could become more significant because the W_R boson mass resolution does not become as wide in the dielectron channel as it does in the dimuon channel. Also, because of its heavy mass, the potential to discover the W_R boson and the heavy neutrino together is much better than in the inclusive search for the new heavy neutrino (assuming the same production mechanism) because of backgrounds.

Figures 9 and 10 show the distributions of the reconstructed invariant masses of the heavy neutrino and W_R boson candidates for signal and background MC samples before and after the selection criteria are applied. All distributions are normalized to 100 pb^{-1} of integrated luminosity. It should be remarked that the trigger efficiency is not included in the plots and tables shown in this section. However, events satisfying all selection criteria would trigger with an efficiency exceeding 95%, as discussed in Section 3.

Background contributions to signal invariant mass spectra could also arise from jets that are misidentified as signal electrons. In principle, such misidentified jets are efficiently suppressed because at least two signal electron candidates are required, but at present this background remains poorly understood because larger statistics of multijet MC, or better, real data, would be necessary to evaluate its contribution reliably. If needed, a better suppression of events with multijets that are misidentified as electrons is possible by applying a more sophisticated isolation energy requirement. The multijet background does not pose a problem in the dimuon analysis, where estimates of the misidentification rate predict a vanishing contribution from multijet to dimuon events.

Finally, the analyses described in this note do not discriminate between same-sign and opposite-sign dileptons. Same-sign dileptons, however, are a very important signature of Majorana neutrinos, which, being their own anti-particles, could decay to a lepton of either charge. The background contribution to same-sign dileptons is much smaller than to opposite-sign dileptons. Of course, both channels would

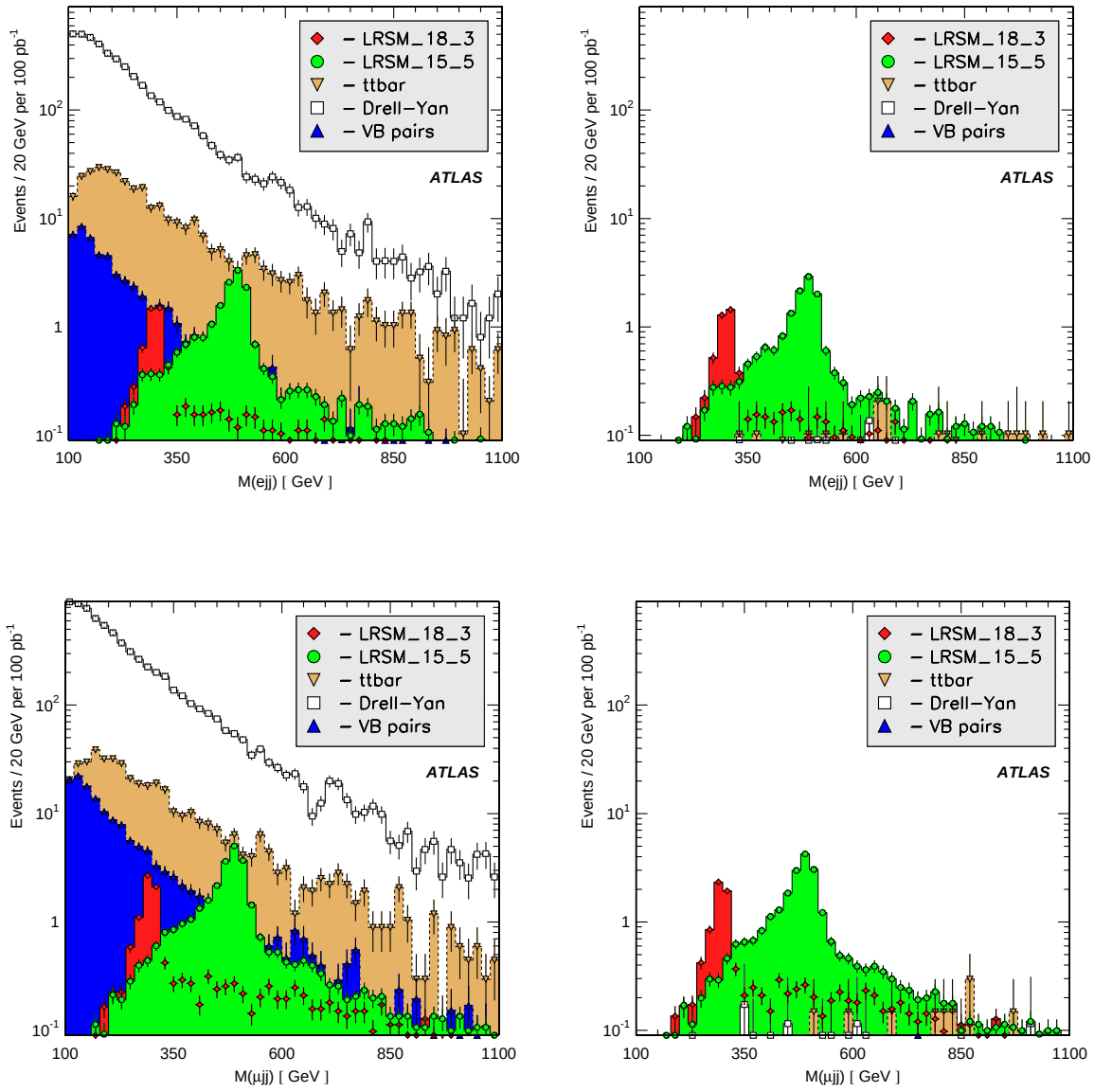

Figure 9: LRSM analysis. The distributions of the reconstructed invariant masses for N_e (top) and N_μ (bottom) candidates in background and signal (LRSM_18_3 and LRSM_15_5) events before (left) and after (right) background suppression is performed in dielectron and dimuon analyses. All distributions are normalized to 100 pb^{-1} of integrated luminosity. LRSM_15_5 and LRSM_18_3 refer to two sets of LRSM mass hypotheses. See the text for more information.

have to be studied if the discovery is made. The studies of charge misidentification performed in the framework of the presented analyses, predict a rate as high as 5% for high-p_T leptons which is strongly η-dependent.

6 Systematic Uncertainties

The following sources of systematic uncertainties have been considered in the described analyses:

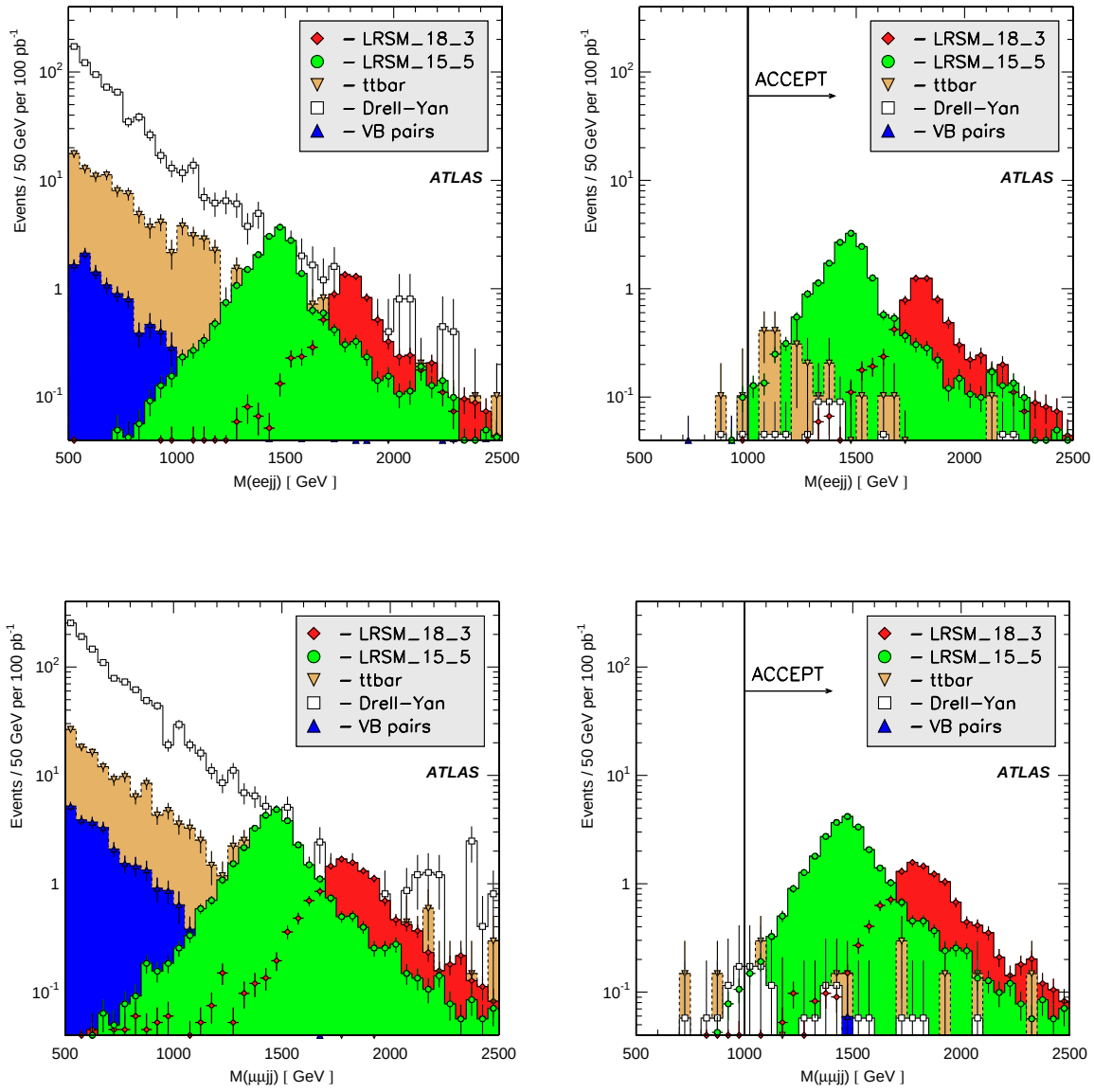

Figure 10: LRSM analysis. The distributions of the reconstructed invariant masses for $W_R \to eN_e$ (top) and $W_R \to \mu N_\mu$ (bottom) candidates in background and signal (LRSM_18_3 and LRSM_15_5) events before (left) and after (right) background suppression is performed in dielectron and dimuon analyses. All distributions are normalized to 100 pb^{-1} of integrated luminosity. Notice that the invariant mass of the W_R boson is shown *before* the requirement $m_{\ell\ell jj} \geq 1000$ GeV is imposed. This variable is strongly correlated with the background-suppressing variables S_T and $m_{\ell\ell}$. LRSM_15_5 and LRSM_18_3 refer to two sets of LRSM mass hypotheses. See the text for more information.

- 20% uncertainty was assumed on the integrated luminosity.
- In the dielectron analyses, 1% was used for the uncertainty in overall trigger efficiency.
- For electron identification and reconstruction efficiency, an uncertainty of 1% was assumed.
- For muon identification, including trigger and reconstruction efficiencies, an uncertainty of 5%

was assumed.

- The uncertainty on the electron energy scale was assumed to be $\pm 1\%$.
- The uncertainty on the muon momentum scale was assumed to be $\pm 1\%$.
- The uncertainty on the jet energy scale was estimated by changing the energies of all jets simultaneously by $\pm 10\%$ and $\pm 20\%$, for $|\eta_{jet}| \leq 3.2$ and $|\eta_{jet}| > 3.2$, respectively.
- The 20% uncertainty in electron p_T resolution was estimated using a Gaussian smearing of p_T with a relative width of $0.66 * (0.10/\sqrt{p_T} \bigoplus 0.007)$, where p_T is in GeV.
- The uncertainty due to muon $1/p_T$ resolution was estimated using a Gaussian smearing of $1/p_T$ with a width of $0.011/p_T \bigoplus 0.00017$, where p_T is in GeV.
- The uncertainty due to jet energy resolution was estimated using a Gaussian smearing of jet energies in such a way that the relative jet energy resolution widens from $0.60/\sqrt{E} \bigoplus 0.05$ to $0.75/\sqrt{E} \bigoplus 0.07$ for $|\eta_{jet}| \leq 3.2$, and from $0.90/\sqrt{E} \bigoplus 0.07$ to $1.10/\sqrt{E} \bigoplus 0.10$ for $|\eta_{jet}| > 3.2$, where E is in GeV.
- Statistical uncertainties on the number of background MC events were considered as systematic uncertainties on the number of background events.
- The systematic uncertainty on the leptoquark cross-section (NLO) [16] was calculated by taking the 40 PDF CTEQ6M tables (two per eigenvector of PDF variations, provided by the CTEQ group for calculating uncertainties [15]), recalculating the leptoquark cross-section with each of these tables, and taking the largest difference of the two variations for each of the 20 eigenvectors to the cross-section calculated with the standard CTEQ6M table. The estimate shown is the sum in quadrature of these 20 differences and the relative difference in cross-section obtained by varying renormalization and factorization scales by a factor of 2. The systematic uncertainty is between 15% and 28% for the tested leptoquark masses.
- The uncertainty of the jet modeling in Z/γ^* events was estimated by comparing the background predictions obtained using MC samples produced with PYTHIA to MC samples produced with ALPGEN. For the leptoquark pair analysis, this results in an uncertainty of about 30% on the background from Z/γ^* events.
- Background cross-sections for $t\bar{t}$ and Z/γ^* processes were assumed to have uncertainties of 12% and 10%, respectively.

Systematic uncertainties affect both signal and background efficiencies, however the significance computation (next section) is mainly affected by the uncertainty on the background. The dominant systematic effects on the background are due to the uncertainties in integrated luminosity (20%), the jet energy scale (16%-35%), jet energy resolution (6%-28%), and the limited statistics of background MC samples (15%-30%). Possible other sources of systematic uncertainties such as initial and final state radiation modeling, or pile-up, were not evaluated. The total systematic uncertainties for signals and backgrounds are summarized in Table 7.

7 Results

The program S_{cp} [29] is used to calculate the significances of possible observations of the signals studied in this note. The significance is defined in units of Gaussian standard deviations, corresponding to the

analysis	effect on signal events		effect on background events	
	1st gen.	2nd gen.	1st gen.	2nd gen.
leptoquark	$\pm$27%	$\pm$29%	$\pm$53%	$\pm$51%
LRSM	$\pm$23%	$\pm$25%	$\pm$45%	$\pm$40%

Table 7: Summary of total systematic uncertainties (%) for 100 pb^{-1} luminosity.

Leptoquark mass	Expected luminosity needed for a 5σ discovery	
	1st gen.	2nd gen.
300 GeV	2.8 pb^{-1}	1.6 pb^{-1}
400 GeV	11.8 pb^{-1}	7.7 pb^{-1}
600 GeV	123 pb^{-1}	103 pb^{-1}
800 GeV	1094 pb^{-1}	664 pb^{-1}

Table 8: The integrated luminosities needed for a 5σ discovery of 1st and 2nd gen. scalar leptoquarks for different mass hypotheses.

(one-sided) probability of observing a certain number of events exceeding the MC-predicted background N_b at a given integrated luminosity. This probability is usually referred to as $CL_b(N)$, where N is the number of observed events. We report the 5σ discovery potential evaluated in terms of $CL_b(N_s+N_b)$, where N_s is the expected number of signal events. Systematic uncertainties in the number of background events were also included in the significance calculations. For second generation leptoquarks, the signal selection was optimized at each mass point to minimize the cross-section times branching ratio needed to reach a 5σ discovery, while for all other analyses the selection cuts presented in earlier sections were used.

The overall reconstruction and trigger efficiencies discussed earlier are used to estimate ATLAS' sensitivity and discovery potential for the studied final states below. These estimates include the trigger efficiency for signal and background events, as discussed in Section 5, Table 2.

7.1 Leptoquarks

The integrated luminosities needed for a 5σ discovery of the 1st and 2nd generation scalar leptoquark signals are shown in Table 8 as function of leptoquark mass, assuming $\beta = 1$. Also, Fig. 11 predicts the integrated luminosities needed for a 400 GeV leptoquark mass discovery, with various values of β^2, at a 5σ level.

Finally, Fig. 12 shows the minimum β^2 that can be probed with ATLAS with 100 pb^{-1} of integrated luminosity as a function of leptoquark mass. Lighter leptoquark masses can be probed with a smaller β because of their larger cross-section. It is evident from this figure that ATLAS is sensitive to leptoquark masses of about 565 GeV and 575 GeV for 1st gen. and 2nd gen., respectively, at the given integrated luminosity, provided leptoquarks always decay into charged leptons and quarks.

7.2 Left-Right Symmetry

The significances of studied signals versus integrated luminosity are shown in Fig. 13. Figure 14 shows the product of signal cross-section and dilepton branching fraction versus the integrated luminosity necessary for a 5σ discovery.

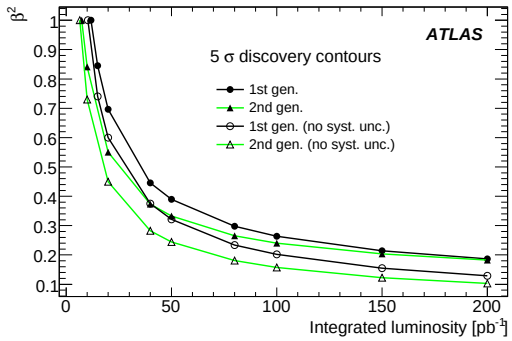

Figure 11: 5σ discovery potential for 1st and 2nd gen. $m = 400$ GeV scalar leptoquarks versus β^2 with and without background systematic uncertainty included.

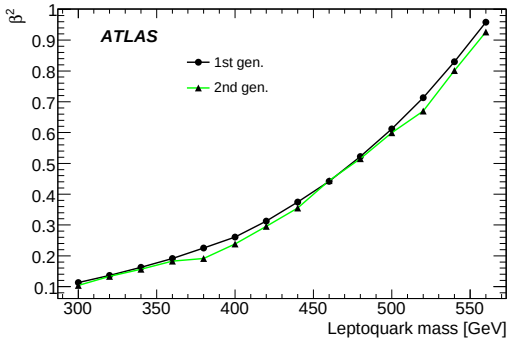

Figure 12: Minimum β^2 of scalar leptoquarks versus leptoquark mass for 100 pb^{-1} of integrated luminosity at 5σ (background systematic uncertainty included.)

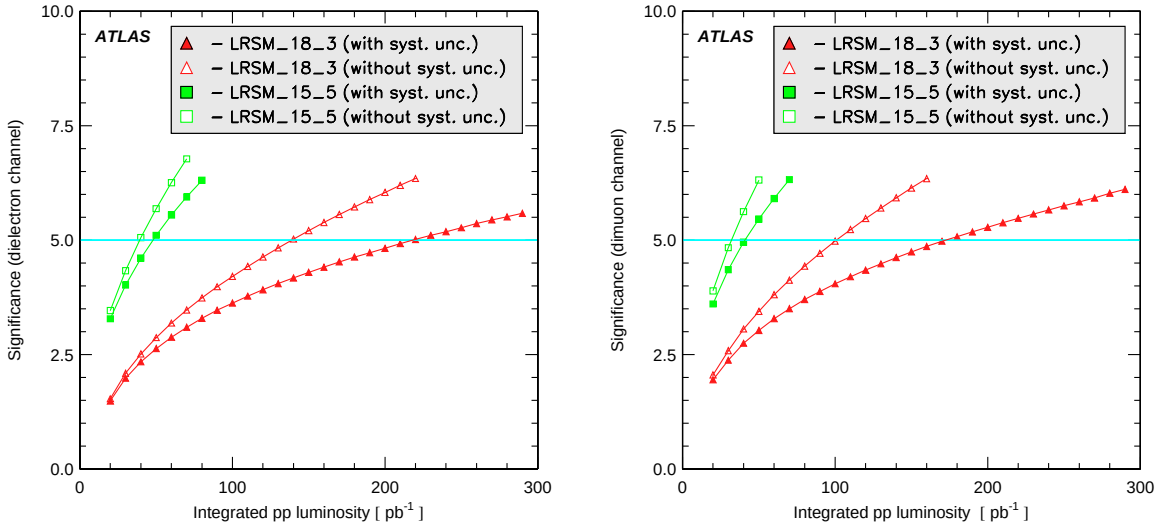

Figure 13: LRSM analysis. Expected signal significances versus integrated luminosity for N_e, N_μ neutrino and W_R boson mass hypotheses, according to signal MC samples LRSM_18_3 and LRSM_15_5. Open symbols show sensitivities without systematic uncertainties. Sensitivities shown with closed symbols include an overall relative uncertainty of 45% (40%) estimated for background contributions in the dielectron (dimuon) analysis. LRSM_15_5 and LRSM_18_3 refer to two sets of LRSM mass hypotheses. See the text for more information.

The overall relative systematic uncertainties on Drell-Yan and $t\bar{t}$ backgrounds are approximately 45% and 40% in the dielectron and dimuon analyses, respectively. These estimates are dominated by contributions from jet reconstruction, uncertainty in integrated luminosity and insufficient MC statistics. Currently, multijet background is poorly understood and is not included in the presented sensitivity estimates for the dielectron channel.

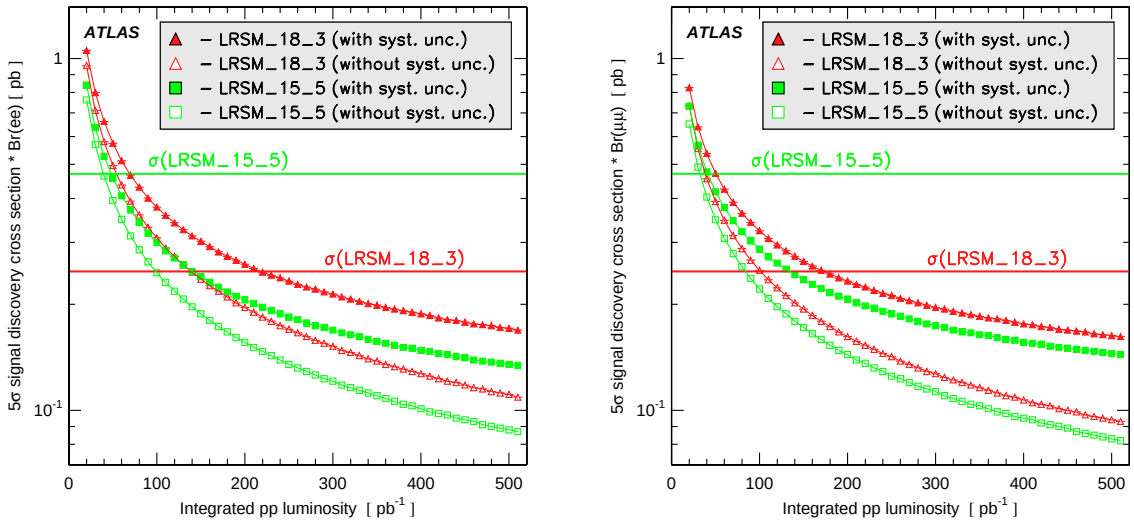

Figure 14: LRSM analysis. The product of signal cross-section and branching fraction to dielectron and dimuon final states versus integrated luminosity necessary for a 5σ discovery. N_e, N_μ neutrino and W_R boson mass hypotheses are for signal MC samples LRSM_18_3 and LRSM_15_5. Horizontal lines indicate nominal cross-sections for two signal MC samples, according to the LRSM implementation in the MC simulation. Open symbols show discovery potentials without systematic uncertainties. Discovery potentials shown with closed symbols include an overall relative uncertainty of 45% (40%) assumed for the background contribution in the dielectron (dimuon) analysis. LRSM_15_5 and LRSM_18_3 refer to two sets of LRSM mass hypotheses. See the text for more information.

8 Summary and Conclusions

Studies of final states with two leptons and multiple jets have been discussed, considering both electrons and muons. The early-data discovery potential for Beyond the Standard Model physics predicted by two prominent GUT-inspired models has been investigated.

Both 1st and 2nd generation scalar leptoquark pair production could be discovered with less than 100 pb^{-1} of integrated luminosity, provided that the mass of the leptoquarks is smaller than 500 GeV and the branching ratio into a charged lepton and a quark is 100%.

Two LRSM mass points ($m_{W_R} = 1.8$ TeV,$m_{N_\ell} = 300$ GeV and $m_{W_R} = 1.5$ TeV,$m_{N_\ell} = 500$ GeV) for the right-handed W_R boson and Majorana neutrinos N_ℓ have been studied in the dielectron and dimuon channels. It was found that discovery of these new particles at these mass points would require integrated luminosities of 150 pb^{-1} and 40 pb^{-1}, respectively.

References

[1] J. C. Pati and A. Salam, *Phys. Rev.* **D10** (1974) 275–289.

[2] E. Eichten, I. Hinchliffe, K. D. Lane, and C. Quigg, *Phys. Rev.* **D34** (1986) 1547.

[3] E. Eichten, K. D. Lane, and M. E. Peskin, *Phys. Rev. Lett.* **50** (1983) 811–814.

[4] W. Buchmuller and D. Wyler, *Phys. Lett.* **B177** (1986) 377.

[5] H. Georgi and S. L. Glashow, *Phys. Rev. Lett.* **32** (1974) 438–441.

[6] M. Leurer, *Phys. Rev.* **D49** (1994) 333–342, arXiv:hep-ph/9309266.

[7] **D0** Collaboration, V. M. Abazov *et al.*, *Phys. Rev.* **D71** (2005) 071104, arXiv:hep-ex/0412029.

[8] **CDF** Collaboration, D. E. Acosta *et al.*, *Phys. Rev.* **D72** (2005) 051107, arXiv:hep-ex/0506074.

[9] **D0** Collaboration, V. M. Abazov *et al.*, *Phys. Lett.* **B636** (2006) 183–190, arXiv:hep-ex/0601047.

[10] **CDF** Collaboration, A. Abulencia *et al.*, *Phys. Rev.* **D73** (2006) 051102, arXiv:hep-ex/0512055.

[11] T. Ahrens, *Boston, USA, Kluwer Acad. Publ.* (2000) . 177p.

[12] R. N. Mohapatra and P. B. Pal, *World Sci. Lect. Notes Phys.* **60** (1998) 1–397.

[13] **D0** Collaboration, V. M. Abazov *et al.*, arXiv:0803.3256 [hep-ex].

[14] T. Sjostrand, S. Mrenna, and P. Skands, *JHEP* **05** (2006) 026, arXiv:hep-ph/0603175.

[15] J. Pumplin *et al.*, *JHEP* **07** (2002) 012, arXiv:hep-ph/0201195.

[16] M. Kramer, T. Plehn, M. Spira, and P. M. Zerwas, *Phys. Rev.* **D71** (2005) 057503, arXiv:hep-ph/0411038.

[17] A. Ferrari *et al.*, *Phys. Rev.* **D62** (2000) 013001.

[18] K. Huitu, J. Maalampi, A. Pietila, and M. Raidal, *Nucl. Phys.* **B487** (1997) 27–42, arXiv:hep-ph/9606311.

[19] K. Melnikov and F. Petriello, *Phys. Rev. Lett.* **96** (2006) 231803, arXiv:hep-ph/0603182.

[20] C. Anastasiou, L. J. Dixon, K. Melnikov, and F. Petriello, *Phys. Rev.* **D69** (2004) 094008, arXiv:hep-ph/0312266.

[21] G. Corcella *et al.*, *JHEP* **01** (2001) 010, arXiv:hep-ph/0011363.

[22] S. Frixione and B. R. Webber, *JHEP* **06** (2002) 029, arXiv:hep-ph/0204244.

[23] R. Bonciani, S. Catani, M. L. Mangano, and P. Nason, *Nucl. Phys.* **B529** (1998) 424–450, arXiv:hep-ph/9801375.

[24] **ATLAS** Collaboration, "Trigger for Early Running." This volume.

[25] **ATLAS** Collaboration, “Reconstruction and Identification of Electrons.” This volume.

[26] **ATLAS** Collaboration, “Muon Reconstruction and Identification: Studies with Simulated Monte Carlo Samples.” This volume.

[27] **ATLAS** Collaboration, “Jet Reconstruction Performance.” This volume.

[28] **ATLAS** Collaboration, “b-tagging performance.” This volume.

[29] S. I. Bityukov, S. E. Erofeeva, N. V. Krasnikov, and A. N. Nikitenko. Prepared for PHYSTATO5: Statistical Problems in Particle Physics, Astrophysics and Cosmology, Oxford, England, United Kingdom, 12-15 Sep 2005.